Examining Dust Emissions and OHV Activity at the ODSVRA

J.A. Gillies, E. Furtak-Cole, G. Nikolich, and V. Etyemezian

Introduction

California State Parks has undertaken ambitious dust control efforts at the ODSVRA to move towards meeting the Stipulated Order of Abatement targets for reducing the mass emissions of PM_{10} from the ODSVRA and lowering the PM_{10} concentrations at key monitoring sites CDF and Mesa2. It is assumed that lowering the total mass emissions and the PM_{10} levels at these two sites indicates that air quality across the Mesa is being improved for all residents.

A recent Report to Parks from DRI (Gillies et al., 2020) presents analysis based on modeling and empirical data, that suggests PM_{10} levels have been lowered by approximately 45% in the vicinity of the CDF monitoring site since dust controls have been emplaced within the riding area of the ODSVRA beginning in 2014. This has been achieved by controlling in 2020, 223 acres using vegetation and temporary wind fencing to reduce dust emissions.

A question that has been posed by stakeholders is: if OHV activity augments the emissivity of the dunes, what fractional increase may this represent? Here we present several lines of evidence that this increase can be defined. The analyses to be reported uses the available PI-SWERL data collected between 2013 through 2020, and the wind and PM_{10} data from the in-Park monitoring network in 2019 and 2020.

PI-SWERL

Since 2013 DRI has undertaken PI-SWERL measurements of PM_{10} emissivity (E, mg m^{-2} s^{-1}) across the ODSVRA in riding and non-riding areas on an annual basis. Measurements have been repeated through time by revisiting locations that were established in 2013, which defined west to east and north to south transects. In addition, over the same period PI-SWERL measurements were also made in the Plover exclosure area during periods when it was and was not accessible. Measurements have also been made in areas where it was deemed critical to obtain data that could be used to, for example, define the change in emissivity as a function of distance past the riding-nonriding boundary on the eastern side of the ODSVRA.

In 2020 OHV activity ceased in April due to restrictions based on health concerns for the transmission of COVID19. The cessation of OHV activity provided an opportunity to investigate how emissivity may change through time due to the absence of OHV. A program was undertaken to repeatedly measure emissivity using the PI-SWERL in the Lagrande Tract at the same geographic positions (30 in number) from April through October (Fig. 1). The positions within the Lagrande Tract selected for repeat measurements were selected from the 2013 transects. A subset of sample locations (62 in number) was also selected that represented the wider riding area domain of the ODSVRA (Fig. 2) to allow comparison with the same locations measured in 2019. The measurement protocols for PI-SWERL have remained the same since 2013 and the testing sequence of RPM and ramping between RPM values used has been the Hybrid3500.

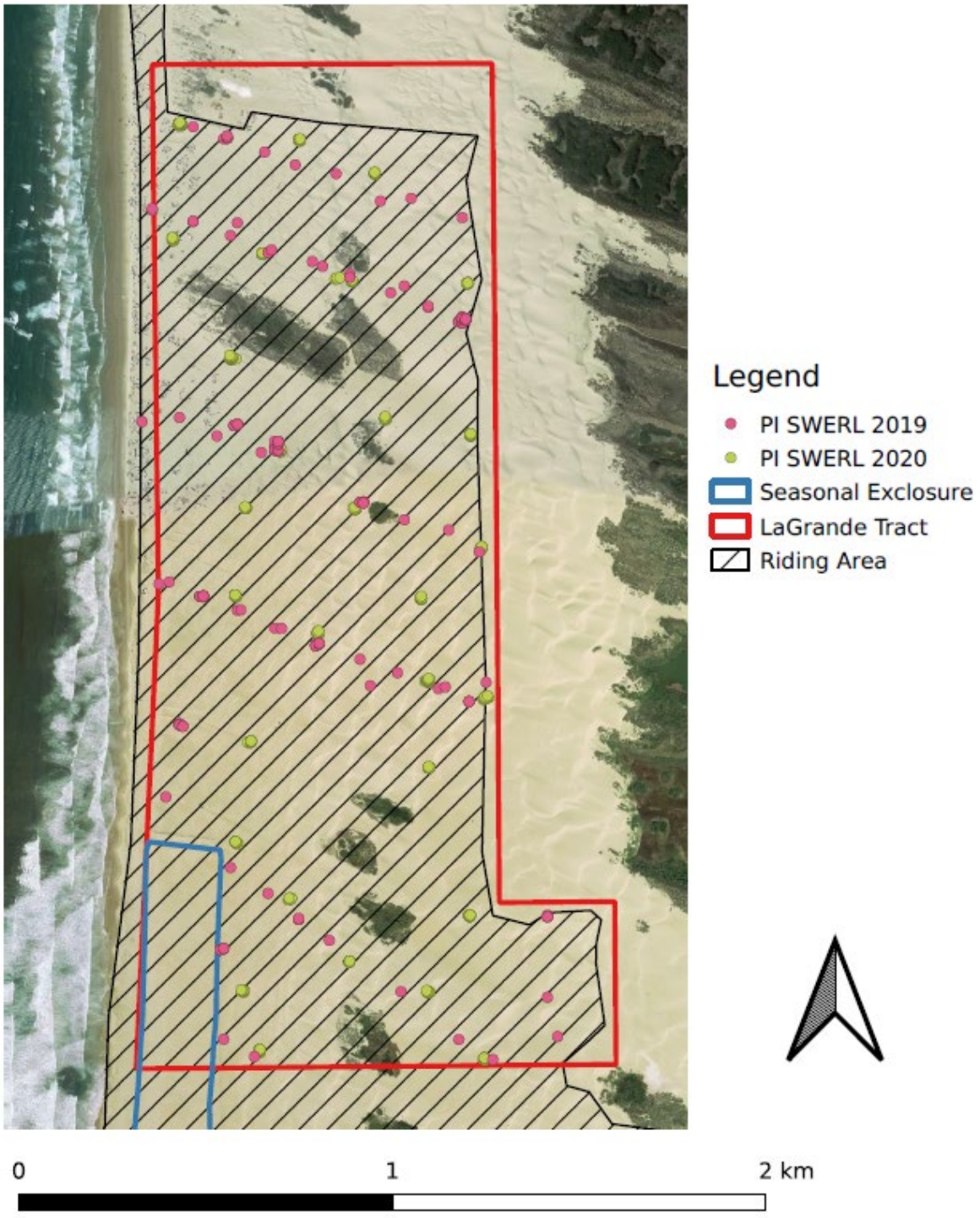

Figure 1. Locations of PI-SWERL tests in the Lagrande Tract in 2019 (pink circles) and in 2020 (green circles).

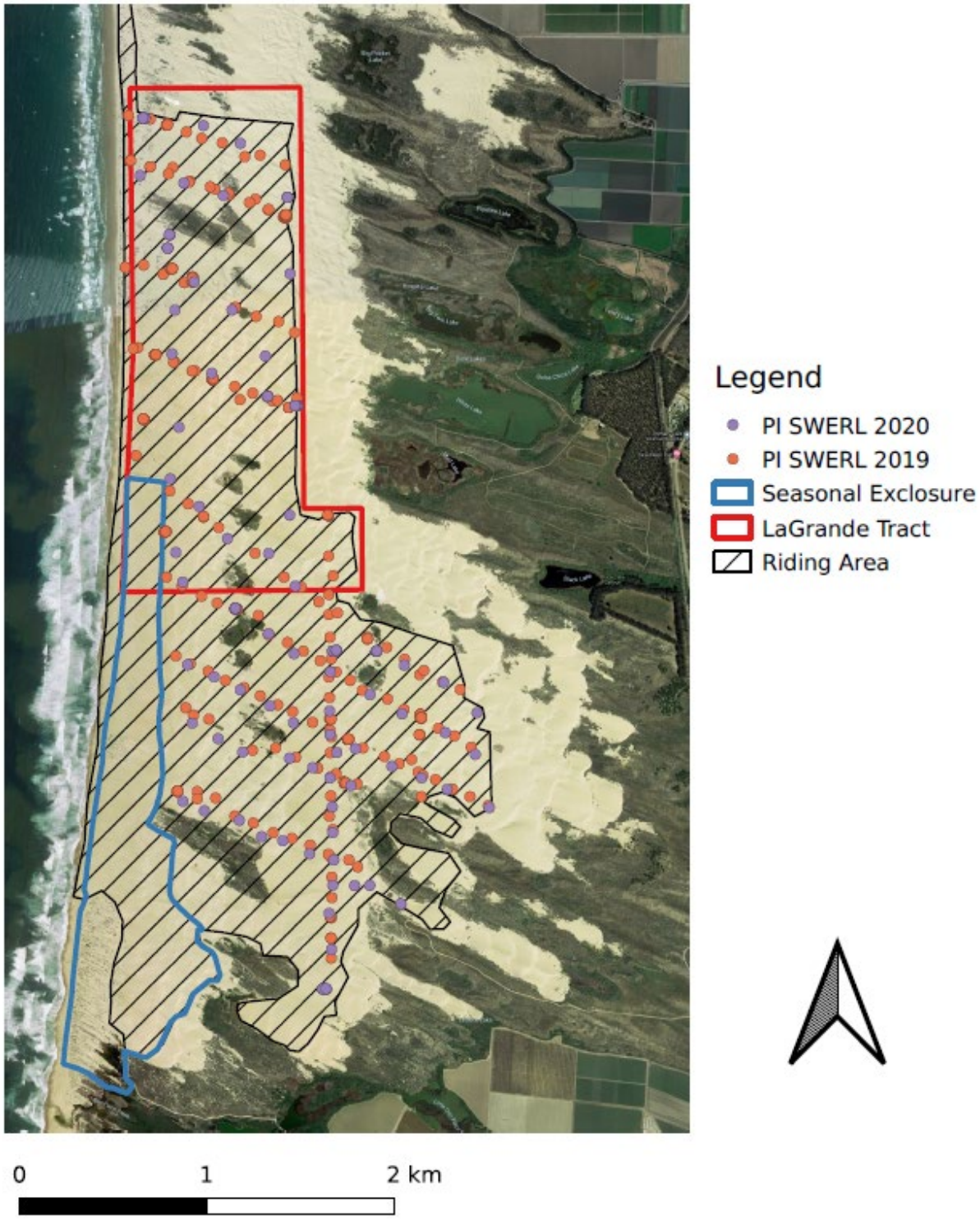

Figure 2. The PI-SWERL test locations for 2020 (purple circles) and 2019 (orange circles).

2013-2019

At the broadest level of comparison of emissivity between riding and non-riding areas the data for all years (2013-2019) can be aggregated together to produce an emissivity and u_* relation for each. For the riding area approximately 932 individual PI-SWERL tests representing the three RPM set points in the Hybrid 3500 test are available. In the same period approximately 317 PI-SWERL tests were made in non-riding areas. These tests do not include those made in the Plover exclosure area between 2013 and 2019.

The mean emissivity (E, mg m^{-2} s^{-1}) as a function of shear velocity (u_*, m s^{-1}) relation for the riding and non-riding areas are shown in Fig. 3. The shear velocity is estimated from the RPM value of the PI-SWERL Hybrid 3500 test sequence using the conversion equation of Etyemezian et al. (2014). An Analysis of Variance (ANOVA) test was conducted on the E values for each of the three sets of u_* values to test whether they are statistically different at the 0.05 level of confidence (i.e., the set P value). The nonparametric ANOVA test was used because these data are not normally distributed. For each of the three u_* values the difference in E between the riding and non-riding tests is statistically significant based on the calculated P values being <0.05 and the F value being greater than the F critical value (generated by the ANOVA test). This demonstrates that the long term mean emissivity of the entire riding area is greater than the long term mean emissivity of the non-riding area for the aggregated data from 2013 to 2019.

These aggregated data sets indicate at the broadest level that, all else being equal, the riding area has a higher emissivity than the non-OHV impacted surfaces, providing some suggestion as to the impact of OHV activity on emissivity. Because the relationship between E and u_* is non-linear (i.e., a power function) the scaling of the OHV effect on emissivity cannot be quantified as a single value. At lower shear velocities (e.g., 0.38 m s^{-1}) emissivity of OHV-impacted sand is enhanced by a factor of 3.6 while at the higher value of 0.61 m s^{-1} it is enhanced by a factor of 1.9 (Fig. 3). OHV activity exerts mechanisms of anthropogenic influence on the dunes throughout the area designated for active riding. The mechanisms consist of rotating vehicle tires that: 1) create a shearing force between sand particles at and near the surface, 2) mix the surface layer of sand, and 3) displace sand particles away from the path of vehicle travel. We hypothesize that these three mechanisms (and perhaps other unidentified near-surface mechanisms) related to OHV activity have the potential to augment the emissivity of the dune sand creating higher concentrations of dust in the air than would occur if this dune system was not impacted by OHV activity.

The mean emissivity relationship for riding and non-riding areas can be disaggregated to examine for geographic influence on the emissivity across space (Fig. 4). For the non-riding area the emissivity data can generally be grouped as: northern dune preserve, areas east of the riding/non-riding boundary in the middle zone of the ODSVRA, and the southern dune preserve. For each of the three zones an ANOVA test was done on the paired data for each PI-SWERL test u_*. The ANOVA tests indicated that the mean emissivity values for each test u_* are significantly different between the geographic locations, with the north having higher emissivity than the east and the south, and east higher than the south (Fig. 5).

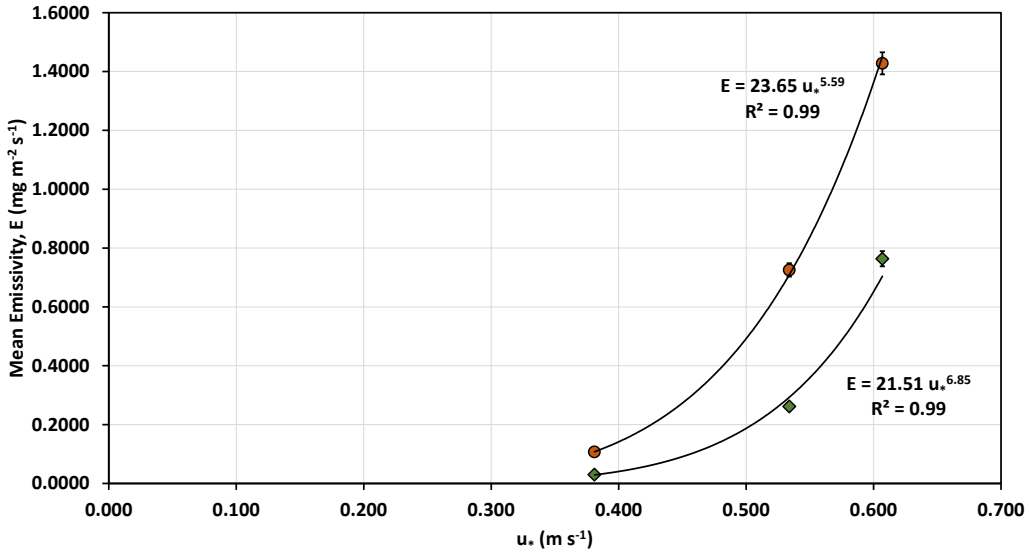

Figure 3. The relation between mean E (mg m^{-2} s^{-1}) and u_* (m s^{-1}) for the amalgamated data from 2013 to 2019 for the riding (orange circles) and non-riding areas (green diamonds). Error bars represent the standard error of the estimate (standard deviation/(#observations-1)$^{0.5}$).

The gradient of increasing emissivity towards the north in the non-riding area also is observed in the emissivity data for the riding area of the ODSVRA. This is demonstrated in Fig. 6, which shows the increase in mean emissivity as a function of latitude bins of 0.005 (decimal) degrees expressed as the factorial increase in emissions when normalized to the southern-most measurement group for all available data (i.e., mean emissivity in latitude bin/mean emissivity in southern-most latitude bin) from 2013 to 2019. This holds for each of the three test u_* values (Fig. 6). In each latitude bin for each test u_*, the emissivity represents the mean of all tests that fall within the bin. This emissivity gradient is a function, in large part, of the gradient in mean grain diameter increasing from north to south. The emission of dust from the dune sands due to saltation is more efficient for sand of smaller mean grain diameter than larger mean grain diameter. This was observed in the analysis of the mean grain size and emissivity data from measurements made in 2013 (Fig. 7).

As identified previously, at the broadest scale the emissivity of the riding area was between 3.6 and 1.9 times greater than the non-riding area for the three PI-SWERL test u_* values. The available data can be interrogated further by pairing specific regions of the riding and non-riding area based on the latitude of the tests. Keeping the non-riding groupings as shown in Fig. 4 and grouping the riding area tests closest in latitude to the non-riding tests, the difference in emissivity can be examined between them along the north to south axis of the ODSVRA. The factorial difference between the riding and non-riding emissivity (i.e., E riding/E non-riding) as a function of north, middle, and southern non-riding latitudinal ranges is shown in Fig. 8. This figure suggests that the difference between the riding and non-riding areas along the north to south gradient is similar for each PI-SWERL test u_* regardless of distance along the gradient. For the lowest test u_* (0.381 m s^{-1}) the difference in emissivity between riding and non-riding is, on average, riding emissivity is 4.3 times greater. For test u_*=0.534 m s^{-1} the factor is 2.7, and for test u_*=0.607 m s^{-1} the factor is 2.0. The lower emissivity of the non-riding area across the north-south

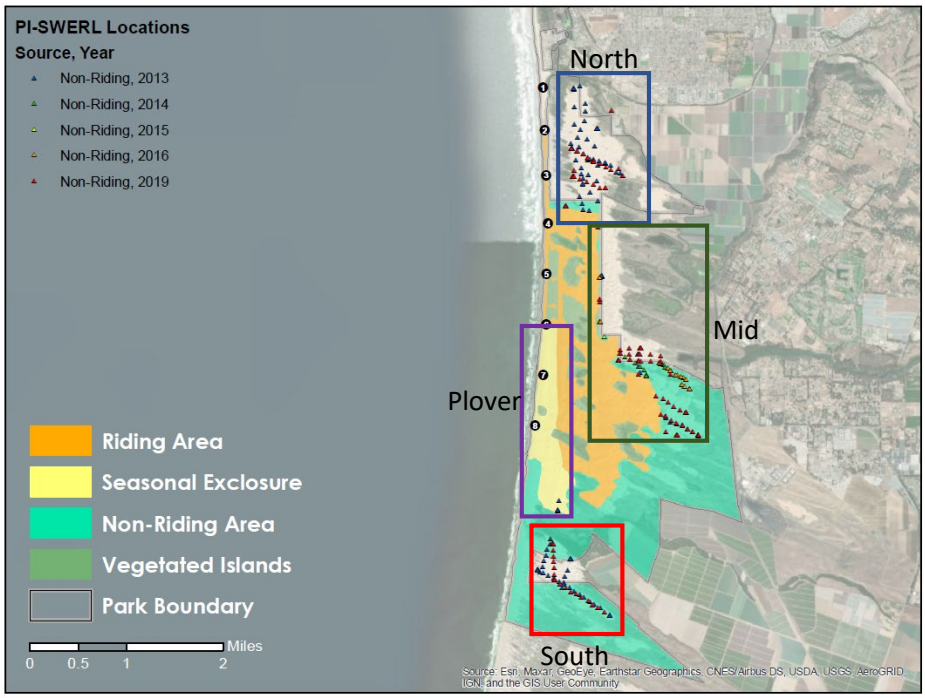

Figure 4. The grouping of the PI-SWERL tests by geographic position in the ODSVRA. In the north west quadrant of the Mid zone, the area east of the non-riding in the ODSVRA is private land and inaccessible for measurements.

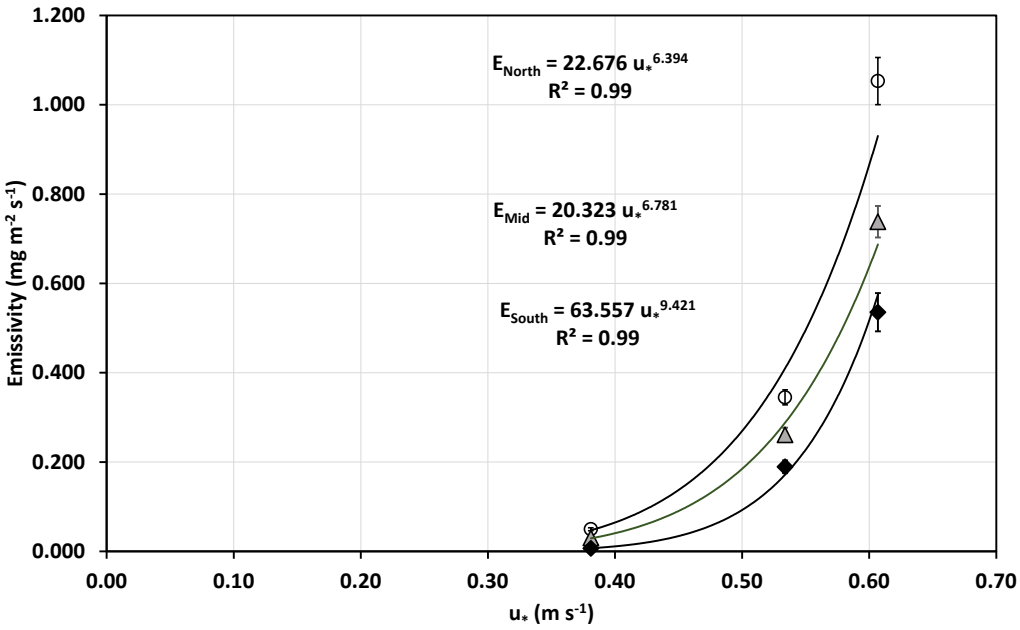

Figure 5. The relation between mean E (mg m^{-2} s^{-1}) and u_* (m s^{-1}) compared by geographic position for the non-riding areas: white circle, north; grey triangle, middle, black diamond, south. Error bars represent the standard error of the estimate (standard deviation/(#observations-1)$^{0.5}$).

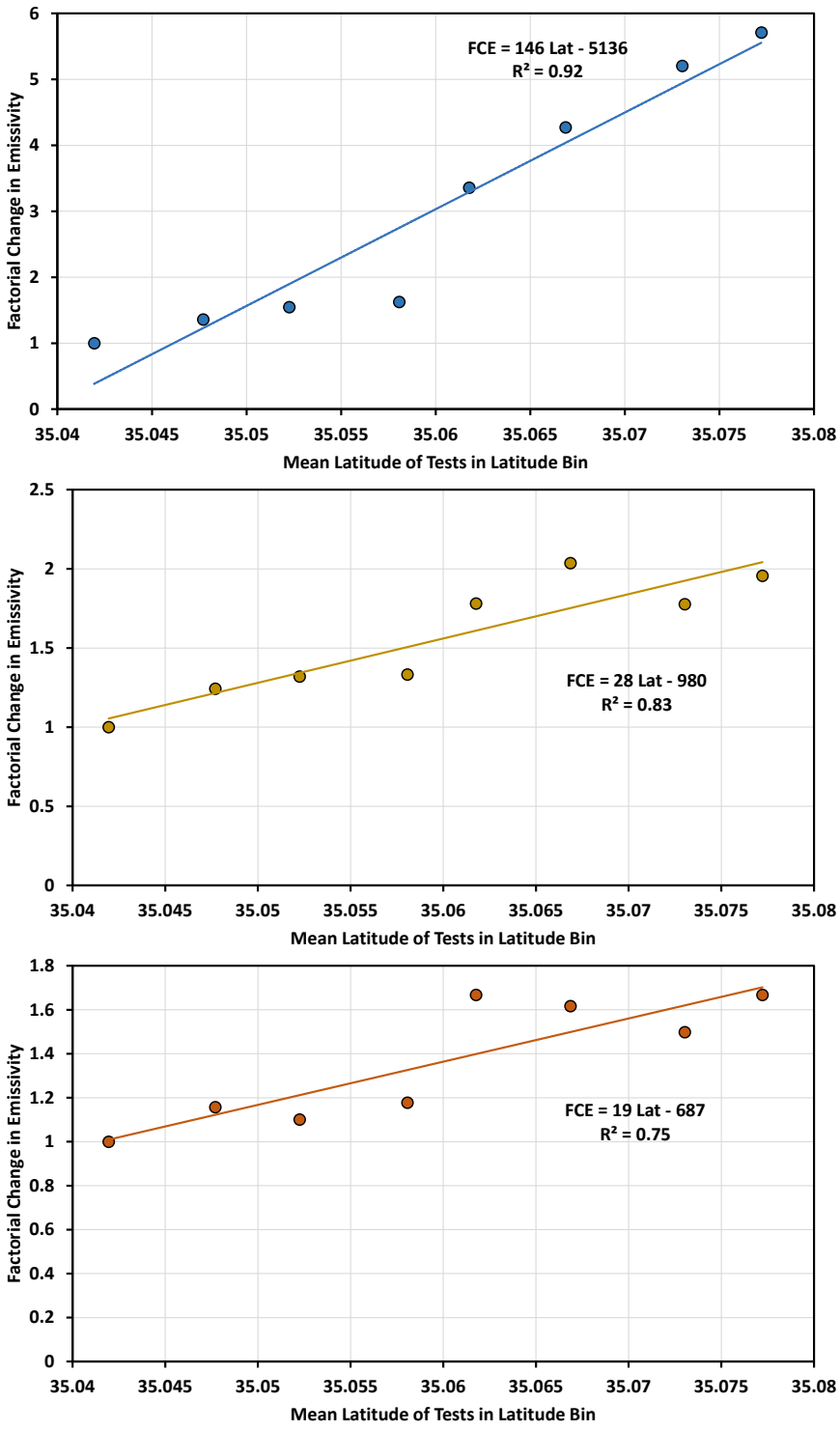

Figure 6. The factorial increase in emissivity as a function of position along the north (35.08 decimal degrees) to south (35.04 decimal degrees) gradient of the PI-SWERL tests in the ODSVRA riding area. Data represent mean emissivity in each latitudinal bin normalized to the mean emissivity in the southern-most latitude bin for the three PI-SWERL u_* values: 0.381 m s^{-1} (top panel), 0.534 m s^{-1} (middle panel), and 0.607 m s^{-1} (bottom panel).

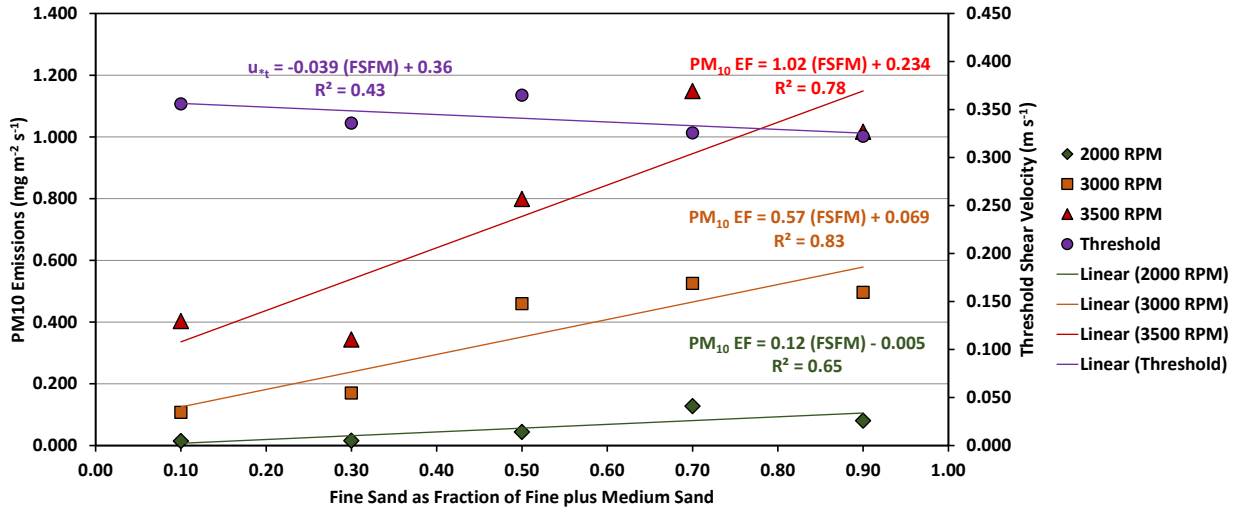

Figure 7. Relationships between PM_{10} emissions and the ratio of fine sand as a fraction of fine sand +medium sand. Data are from 2013 as reported in "Addendum to the Pi-SWERL Report" (Etyemezian et al., 2014, refer to Fig. 15).

distance of the ODSVRA, and the fact that this difference scales consistently as a function of latitude and u_*, suggests this represents, in part, the augmentation of dune sand emissivity due to OHV activity. Unfortunately, there are no data to evaluate if there is a north-south gradient in vehicle activity, which could also be influencing the relation shown in Fig. 8.

2020 Lagrande Tract Repeated PI-SWERL Survey

PI-SWERL tests were repeated within the Lagrande Tract area from April to October 2020 during which time OHV activity was largely prohibited (NB, no measurements were made in August). The locations of the tests remained constant during that time (Fig. 1). It must be recognized that although the positions of the tests remained the same, the sand was intermittently being transported by the wind. The wind redistributes the sand and the bedforms (ripples and dunes) migrate in the direction of the sand transporting wind during transport events. Although the tests were conducted at the same locations, clearly the sand at those locations was not the same sand from the previous tests. The wind essentially randomizes the surface with each transport event and makes comparison of emissivity at a particular position questionable. For these data it is more reasonable to aggregate them by creating a mean emissivity for the tests made during set periods of time, for example by month.

In addition to the randomization of the surface by the wind, moisture conditions due to precipitation dew and fog varied across space and through time during the PI-SWERL testing. This creates a degree of difficulty for comparing emissivity as a function of time and requires that some aggregation of the data be undertaken to try and account for the variability, particularly due to moisture effects. Ideally the data would be aggregated by a moisture-based criterion, but a reliable metric and measurement method remains to be developed.

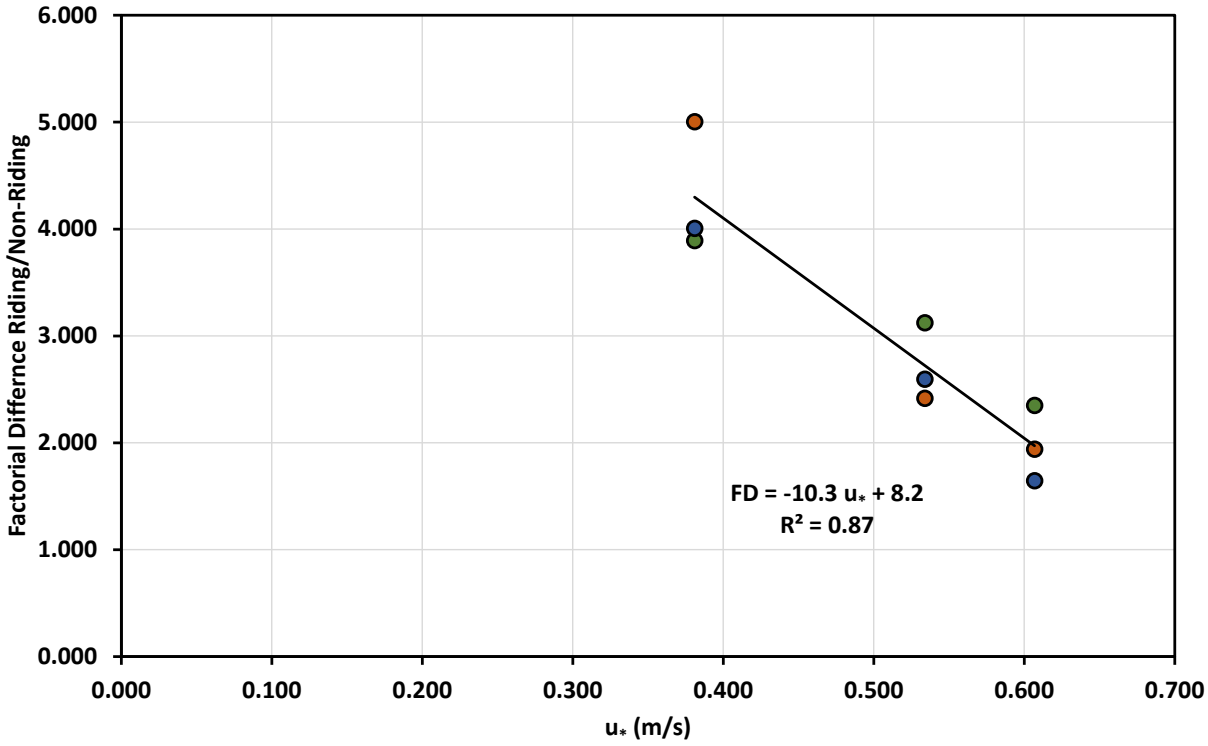

Figure 8. The factorial difference in emissivity between riding and non-riding areas as a function of PI-SWERL test u_* and as a function of the latitudinal range of the northern (blue circles), middle (green circles) and southern (orange circles) non-riding area groupings.

The mean emissivity and u_* relations for the Lagrande Tract for April, May, June, and July are represented by color-coded circles in Fig. 9. For comparison they are plotted along with the mean emissivity and u_* relations for the Lagrande Tract in 2019 (for tests in the same area as 2020), all riding area tests (2013-2019), and all non-riding tests (2013-2019). These data show that in April 2020, the emissivity is most similar to the mean non-riding area relationship, likely due to moisture effects linked with precipitation events in April 2020. In May and June 2020, the emissivity is similar to the emissivity in the same general area as was measured in 2019, differing by less than a factor of 1.5 for the two highest shear velocities in the PI-SWERL test. In July 2020, the emissivity is most like the mean non-riding area relationship based on PI-SWERL testing between 2013 to 2019. The factorial difference (i.e., E-2019/E-2020 for the same test u_* values) between emissivity for 2019 and 2020 for April through October for the same area of the Lagrande Tract where measurements were made in 2020 is shown in Fig. 10. In general, the emissivity of the Lagrande Tract in 2020 was less than in 2019. The month to month pattern of change in emissivity illustrated in Fig. 10, could, in part, be due to moisture effects from precipitation, fog and dew events. The lower emissivity in 2020 may also be indicative of changes in the sand due to the cessation of riding, caused by, for example, removal of the PM_{10} source material by winnowing, coarsening of the sand near the surface due to wind-driven sorting processes, and the cessation of the mixing of the surface sand by vehicle tires.

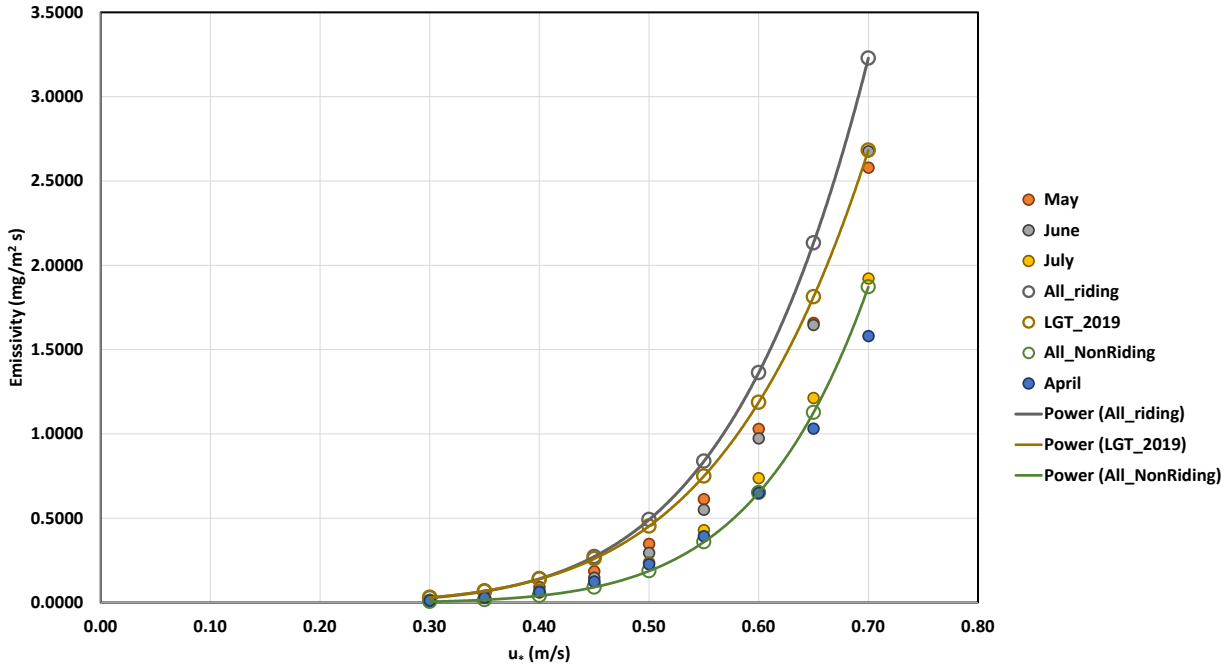

Figure 9. The mean emissivity and u_* relations for the Lagrande Tract for April, May, June, and July 2020 compared with Lagrande Tract 2019, all riding area (2013-209), and all nonriding area (2013-2019).

2020 Compared to 2019 for Areas Outside the Lagrande Tract

In May 2020 PI-SWERL measurements were made across the ODSVRA riding area that represent a sub-set of the sampling grid that was established in 2013 (Fig. 2). These measurements were made between May 12 to May 17. The mean emissivity measured in 2020 for the three test u_* values were compared to the emissivity data from PI-SWERL testing in May 2019 to evaluate if a significant change in emissivity had occurred across a larger spatial domain than just the Lagrande Tract. An ANOVA test for each of the test u_* values between the two years was carried out and the results show that the mean emissivity in 2020, E=0.064 mg m^{-2} s^{-1} for u_*=0.381 m s^{-1} (RPM=2000), was not different than the mean value of E=0.075 mg m^{-2} s^{-1} for 2019. For the higher test u_* values of 0.534 m s^{-1} (RPM=3000) and 0.607 m s^{-1} (RPM=3500), the mean E values in 2020 were 0.324 mg m^{-2} s^{-1} and 0.831 mg m^{-2} s^{-1}, respectively, while for the 2019 data they were 0.503 mg m^{-2} s^{-1} and 1.037 mg m^{-2} s^{-1}, respectively. ANOVA testing for each pair indicate that the E values are significantly different for the higher u_* test values between the two years. This indicates that the mean emissivity of the riding area as a function of u_* in May 2020 (Fig. 11) was lower than in 2019, as was also observed for the Lagrande Tract repeat survey area. This could be a result of the cessation of OHV activity, but it could also be due to the effects noted in the previous section.

Due to constraints due to weather and accessibility, PI-SWERL measurements in the nonriding areas were extremely limited in 2020. Comparison with 2019 measurements could not be made.

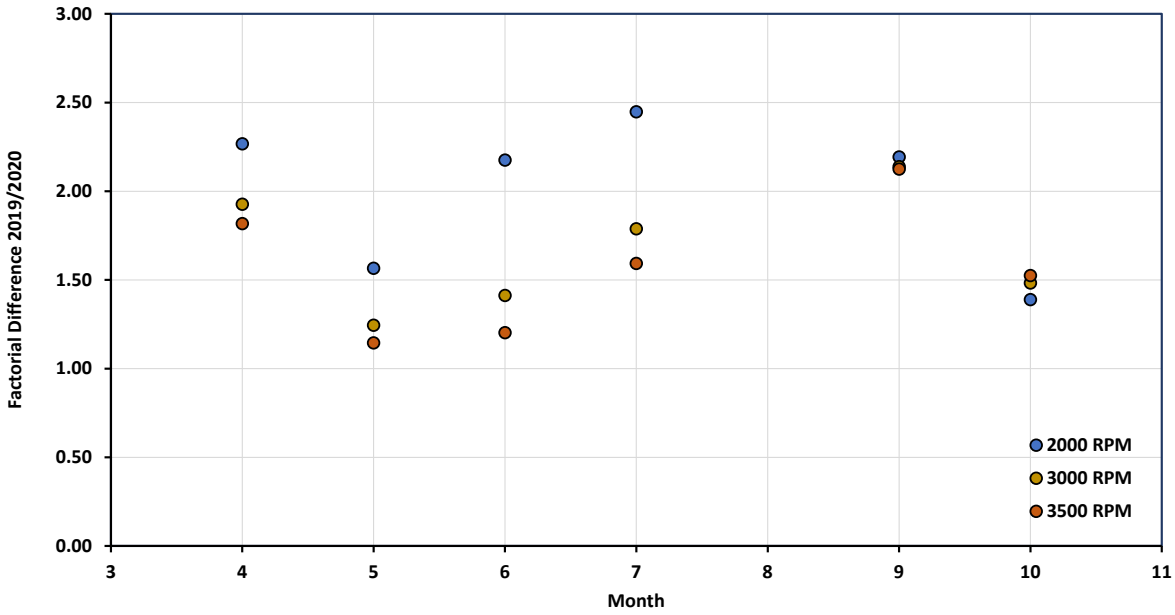

Figure 10. The factorial difference in mean emissivity between 2019 and 2020 for each PI-SWERL test u_* (RPM) from April (month 4) through September (month 10).

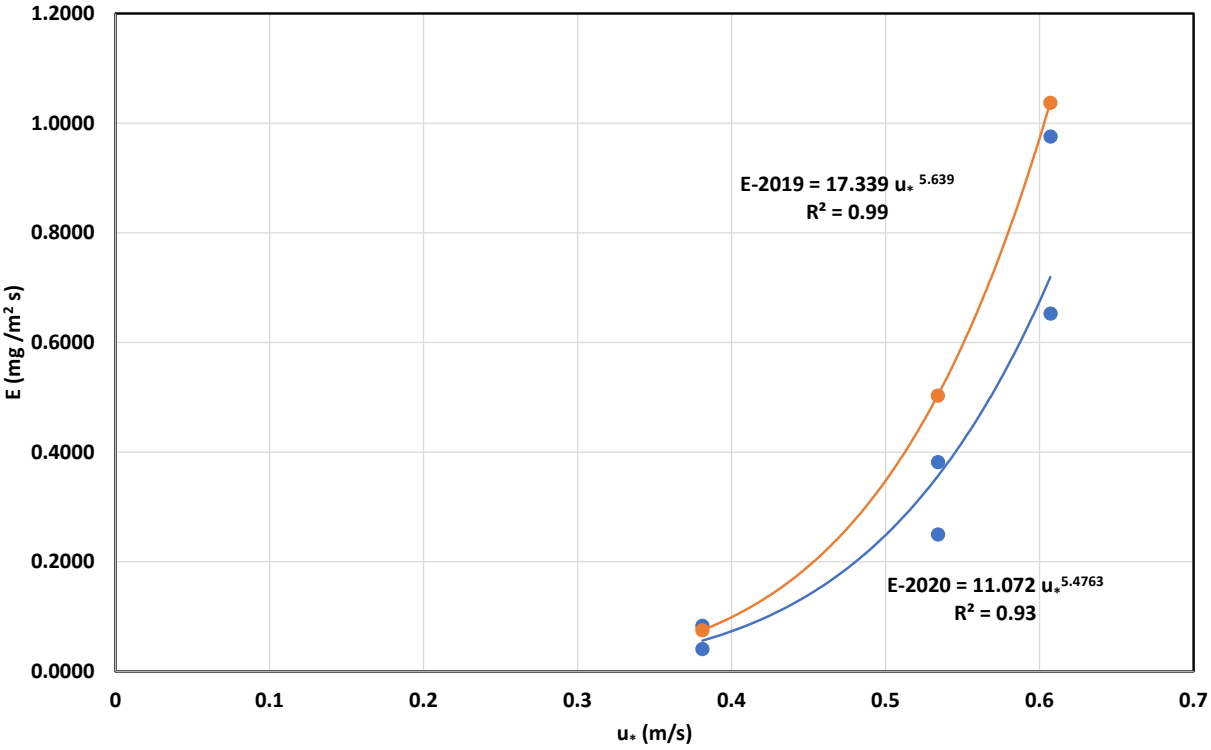

Figure 11. The mean emissivity and u_* relations for the ODSVRA in May 2019 (orange circles) and May 2020 (blue circles).

PM Concentration and Wind Data from the In-Park Monitors, 2019-2020

During 2019 and 2020, a meteorological and airborne dust monitoring network (Fig. 12) consisting of 15 monitoring locations was installed at the ODSVRA in active riding areas, at the eastern border of the Park, and exterior to the Park on Philips 66 land and at the CDF monitoring site. These monitoring networks served to characterize wind conditions and the distribution of airborne particulate matter (PM) during wind events exceeding the threshold wind speed for saltation that contribute to elevated concentrations of PM_{10} (particulate matter ≤10 micrometers in aerodynamic diameter). Data from 2019 and 2020 derived from the in-Park monitoring network allow for an examination of PM_{10} and wind relations across a wide area of the ODSVRA and to examine for changes in the dust emission system through time.

The wind speed and direction data at these sites are measured with the MetSense instrument, which uses 2-D sonic anemometry to derive these parameters. Particulate matter at each station is measured using a MetOne Instruments 212-2 Particle Profiler that measures particle counts in eight size bins. These particle count bins are used to derive a PM_{10} concentration on a minute and hourly basis. In order to achieve a measure of PM_{10} from this instrument that can be compared between stations and to the PM_{10} measured by an EPA Federal Equivalent Method Beta Attenuation Monitor (BAM), a calibration procedure has been developed to convert the MetOne particle count data to a BAM-equivalent PM_{10} concentration.

The BAM equivalent PM_{10} concentration for each 212-2 instrument is achieved by collocating the 212-2 instruments in an environmentally controlled chamber in a lab at DRI's campus in Las Vegas, NV, and establishing a unit-specific calibration relation. The instruments are rack-mounted in the chamber beside a BAM and a filter-based sampler (US EPA approved cyclone-style sampler). Under controlled

Figure 12. Locations of the meteorological and airborne dust monitoring stations at the ODSVRA and exterior to the ODSVRA.

temperature and humidity conditions dust created by simulated saltation of Oceano Dune sand is generated in the chamber that all instruments are exposed to simultaneously. The data stream (particle counts in each bin size) from the 212-2 units and the BAM (μg m^{-3}) are recorded by a datalogger.

Each 212-2 outputs a data string corresponding to the counts of particles that are greater than a given size in a given volume (0.01667 liters). In order to translate this into a PM_{10} concentration: 1) the number of particles in a size bin is calculated by subtracting the number of counts associated with all larger size bins, 2) a diameter representing all the particles within a size bin is estimated (taken to be the geometric mean of the minimum and maximum of the size bin), 3) the volume of an individual particle of the characteristic diameter of the size bin is calculated assuming particles are spheres, 4) the total volume of particles in a volume of air is calculated by multiplying the volume of a single particle by the number of particles in the size bin in the known volume of air, and 5) a particle density of 2600 kg m^{-3} is used to estimate the mass concentration of particles in the size bin. The cumulative mass concentration of particles through size bin 6 is denoted as PMbin6. A calibration relationship between the BAM and the PMbin6 value is defined through the paired values of BAM-measured PM_{10} and calculated PMbin6 for each 212-2 instrument. Hereafter the measurements made with the 212-2 and corrected with the calibration relationships will be identified as 212-PM_{10}. An example of this relationship is shown in Fig. 13. The consistency of the calibration relations among the 212-2 units as measured in March 2020 was quite good. The mean slope value for all units combined was 4.106 (±1.100) and mean intercept was -4.741 (±3.514). The mean correlation coefficient was 0.950 (±0.013).

In addition to the chamber testing, an in-Park calibration station was established in 2020. This station consisted of a BAM, mounting hardware for two 212-2 units, wind speed, wind direction and RH instruments, and datalogging with modem telemetry. The purpose of the in-Park calibration was to determine the performance of the 212-2 and BAM instruments under ambient conditions at the ODSVRA. Of concern was their ability to perform under high wind conditions and whether this resulted in a bias in the measurement compared to the BAM. In 2020, 10 of the 212-2 units were collocated with the in-Park BAM. The available data from the in-Park calibration testing indicates that the 212-2 units were not adversely affected by wind speeds that exceeded 5 m s^{-1} compared to the chamber conditions (i.e., no wind). The mean slope value and intercept values were 4.481 (±0.889) and -8.332 (±24.605), respectively. The mean correlation coefficient was 0.917 (±0.119). The differences in slope, intercept, and correlation coefficient are due to the dynamic nature of the field environment, but the degree of change indicates that under these conditions the correlation between the two instruments remained high and provides confidence that the 212-2 performs well at the ODSVRA. In this report, because we do not have in-Park calibrations for all relevant stations, the PMbin6 data are converted to 212-PM_{10} using the March 2020 chamber derived relationships for each 212-2 unit. The analysis to be presented is based largely on the use of ratio values so the absolute values of 212-PM_{10} may not match the actual values. Using the 212-2 chamber-derived calibration coefficients ensures the inter-comparisons among the different units can be made with confidence, as differences in 212-PM_{10} measurements are not due to a mixing of calibration methods, i.e., in-lab versus in-Park.

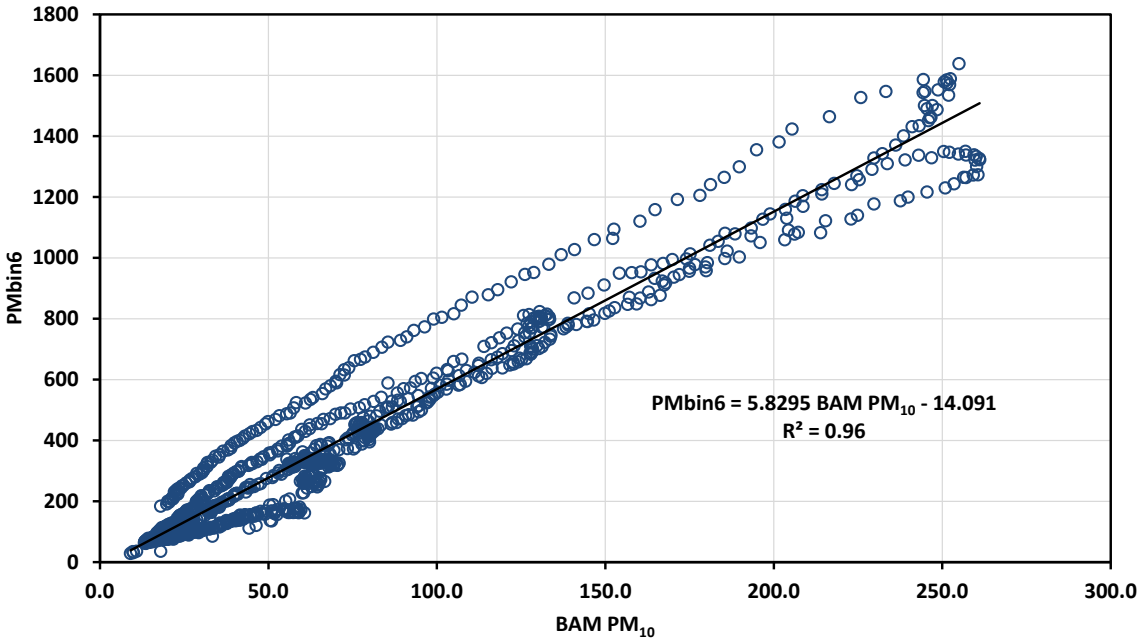

Figure 13. An example of the calibration relationship between BAM and PMbin6 from chamber testing.

Of key interest in 2020 due to the closure of the riding area to OHV activity is whether a change in the observed PM_{10} levels as measured by the in-Park monitoring network is observed for similar wind conditions through time. As previously reported in Etyemezian et al. (2019), the in-Park PM_{10} monitoring data suggest a changing pattern in the emissions between April and August based on analysis of the 2017-2018 data. These data suggested that the magnitude of the wind speed that was required to reach the observed concentrations of dust decreased as the months progressed from April to August. That is, for comparable wind speeds, PM_{10} concentrations were higher during later months (August) than earlier in the season (May-July), which suggests the emissivity of the surface had increased with time in this period.

Based on recent reports by Furtak-Cole and Gillies (2020) and Gillies et al. (2020), a different analytical approach than was used by Etyemezian et al. (2019) was used for the 2019 and 2020 in-Park monitor data (i.e., stations located on sand) to evaluate if the pattern of PM_{10} concentrations through time as described by Etyemezian et al. (2019) was repeated in 2019 and 2020. The list of these stations and their latitude/longitude are provided in Table 1. In this report the method of Furtak-Cole and Gillies (2020) and Gillies et al. (2020) using total of wind power density (WPD, W m^{-2}) and total 212-PM_{10}, and the calculation of the T212-PM_{10}:TWPD ratio has been adopted. This ratio can be used as a metric to evaluate changes in the dust emission system across the sampling domain and through time. Recall, WPD is defined as (e.g., Kalmikov, 2017):

$$WPD=0.5\ \rho_a\ u^3 \quad (1)$$

where ρ_a is air density (kg m^{-3}), and u (m s^{-1}) is wind speed at a given height above ground level (AGL) common to all sites. For the in-Park monitors the wind speed measurement height was 3 m. The ratio of total PM_{10}:total WPD serves as a metric to evaluate how the dust emission system is changed by

Table 1. The station names and position data for the PM and met monitoring stations. Stations shaded gray are not surrounded by sand or are outside the ODSVRA.

Station Name	Latitude	Longitude
Moymell	35.0751	-120.6199
BBQ	35.0700	-120.6197
Lagrande	35.0664	-120.6197
Camping	35.0662	-120.6218
Foredune	35.0650	-120.6264
Windfence	35.0644	-120.6221
Acacia	35.0605	-120.6205
Cottonwood	35.0597	-120.6190
Haybale	35.0535	-120.6016
Phillips66	35.0489	-120.5939
Scout	35.0482	-120.6032
Tabletop	35.0478	-120.6168
CDF	35.0467	-120.5877
Pipeline	35.0406	-120.6180
Sodar	35.0368	-120.5962

changes to or in the landscape. With no changes to the surface where the emissions originate from, this ratio will reflect the efficiency of the wind and saltation system to produce PM_{10} for the prevailing environmental conditions during the period of interest. If, however, the surface from which the emissions are originating from is changing, for example, by removal of the PM_{10} source material or coarsening of the surface sand (i.e., increasing mean grain diameter), the ratio should diminish as dust production by saltation processes becomes less efficient in producing PM_{10} dust. There is a limit to the explanatory power of this ratio, which is that if winds are at or close to the designated threshold speed either at the monitoring location or in the source area for a large part of the record, the value becomes unstable due to a potential paucity of data but also because as wind speed diminishes the strength of the coupling between the wind and the saltation-generated PM_{10} weakens and is subject to influence of PM_{10} from other sources.

In the analysis presented here only one filter is applied to the data, that wind speed measured at 3 m above-ground-level be ≥5 m s^{-1}, which for most cases will be above the wind speed across the domain that will cause the sand to saltate and emit dust-sized particles. Total WPD for a month is the sum WPD for all hours that meet the wind speed filter criterion. Total 212-PM_{10} for the month is the sum of T212-PM_{10} for each hour that met the wind speed criterion. This was done to produce a stable ratio of total PM_{10}:total WPD. As the in-Park stations of interest are surrounded by sand that can emit dust whenever the wind exceeds the threshold for transport regardless of wind direction, we chose not to filter for wind direction.

For each of the in-Park stations (see Table 1) the relation between T212-PM_{10} and TWPD as a function of month was derived for 2019 (May/June through September) and 2020 (April through August). For all stations in both years this relation was highly correlated. Examples of this relation for stations Moymell, Windfence, Scout, and Tabletop for 2019 are shown in Fig. 14. Examples of this relationship for the same stations for 2020 are shown in Fig. 15. These examples span the north-south distance of the in-Park stations. As the T212-PM_{10} and TWPD relation is highly correlated for all stations in both years the T212-PM_{10}:TWPD ratio can be used to examine if the dust production due to wind-driven saltation

changes across space and through time. The mean number of hours in each month above the threshold WPD of 77 W m^{-2} for calculating TWPD and T212-PM_{10} ranged from 72 (April 2019) to 116 (September 2019).

In 2019 the in-Park stations did not all begin collection in the same month with stations coming on line in either May or June. To demonstrate how the T212-PM_{10}:TWPD ratio changed through time in 2019, this ratio as a function of month for the same four stations shown in Fig. 14 is shown in Fig. 16. The examples of the change in the T212-PM_{10}:TWPD ratio as a function of month shown in Fig. 16, suggest that, as Etyemezian et al. (2019) noted, higher PM_{10} concentrations are observed in the late summer month of August compared with previous months for similar wind conditions. These plots indicate that as time progressed the dunes were producing higher concentrations of PM_{10} for lower, but above threshold wind speed because the T212-PM_{10}:TWPD ratio increased through time. To compare among all the in-Park sites and to account for the different time intervals the stations were operational, the T212-PM_{10}:TWPD ratio for each month the station operated was normalized to the ratio estimated for its beginning month of operation for each station (i.e., [T212-PM_{10}:TWPD-month-n]/[T212-PM_{10}:TWPD-month-1]). The mean normalized T212-PM_{10}:TWPD ratio for each increment of month is shown in Fig. 17. When all in-Park stations are considered, the normalized mean T212-PM_{10}:TWPD ratio shows an incremental increase from spring through to fall across the span of the monitoring stations in 2019. In general, the data in Fig. 17 indicate that in 2019, when OHV activity was not restricted, from May to September concentrations of PM_{10} for equivalent WPD increased by ≈48%, or 12% per month.

A further demonstration of the change in concentrations of PM_{10} for equivalent WPD for the Park as a function of time can be demonstrated using the 2017 and 2018 data from the available Met/PM stations operating in those years and calculating the TPM_{10} and TWPD for each available month.

The monthly normalized mean T212-PM_{10}:TWPD ratio (normalized to the initial month of monitoring) for these years is shown in Fig. 18. In both year there is an increase in this ratio from spring to summer, for the in-Park and out-of-Park stations, followed by a decrease into the fall months, similar to the patterns shown for the example stations for 2019 shown in Fig. 14. Note that for the out-of-Park stations compared to the in-Park stations the pattern of change through time is similar, but the absolute value range is not. This is because the height of wind speed measurement at those locations is 10 m, not 3 m, so they are not directly comparable.

The same analyses were carried out for the available 2020 in-Park station data, which operated from April through to early September 2020. The measurement record in September 2020 was not deemed sufficiently long for allowing comparisons with the previous months, so it was not used (# hours >77 W m^{-2} ranged between 3 and 26). The mean number of hours in each month, April to August, above the threshold WPD of 77 W m^{-2} for calculating TWPD and T212-PM_{10} ranged from 69 (August 2020) to 173 (May 2020). Examples of the T212-PM_{10}:TWPD relation for stations Moymell, Windfence, Scout, and Tabletop for 2020 as a function of month are shown in Fig. 19. The plots in Fig 19 suggest that in 2020, concentrations of PM_{10} due to saltation of dune sand within the ODSVRA changed substantially compared to 2019, and the general pattern of emissions increasing incrementally through the summer months first noted by Etyemezian et al. (2019) and repeated again in 2019 does not hold. Using all the available in-Park stations (Table 1) for 2020, the mean normalized T212-PM_{10}:TWPD ratio was estimated by normalizing to the ratio for April (Fig. 20). The relation shown in Fig. 20 indicates that across the spatial domain of the PM and meteorological monitoring network, the concentrations of Total PM_{10}

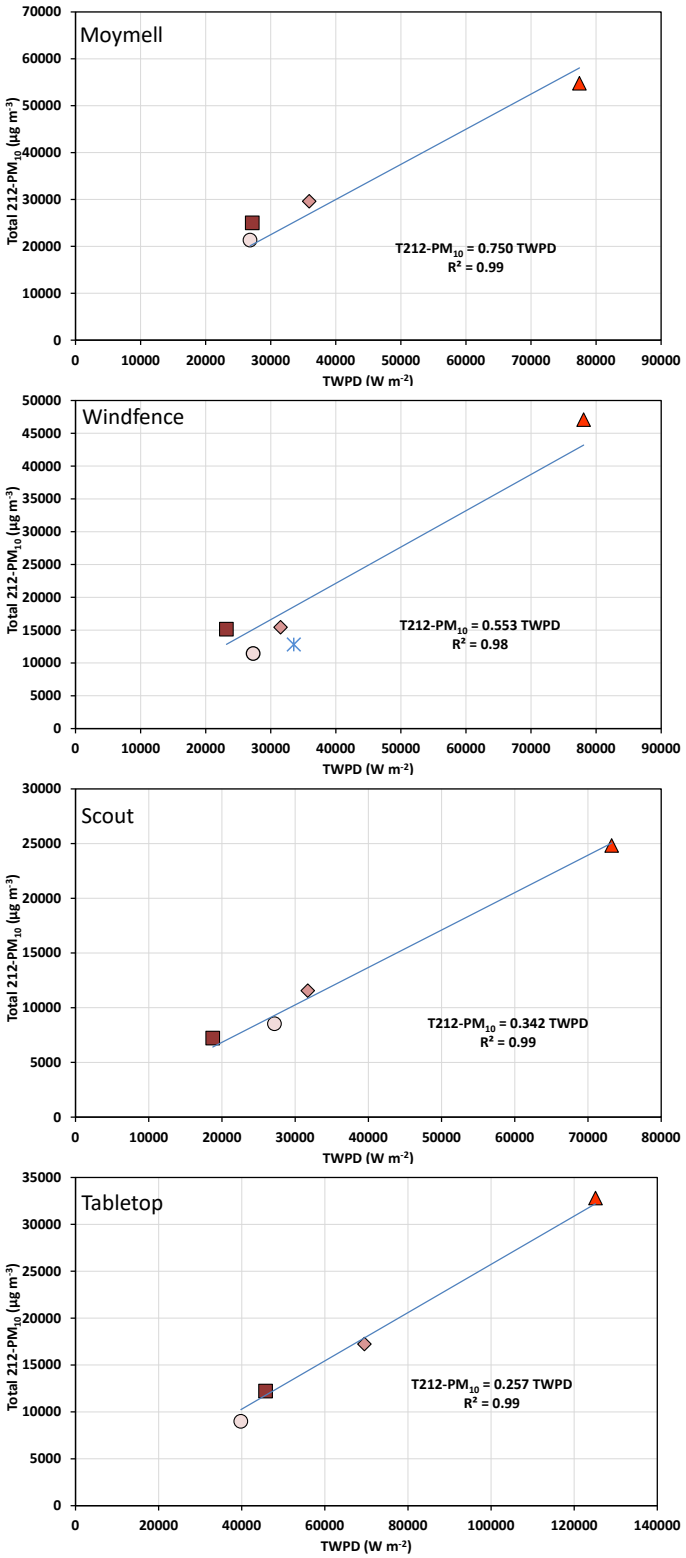

Figure 14. Examples of the T212-PM_{10} and TWPD relation for stations Moymell, Windfence, Scout, and Tabletop for 2019. Shape/color indicates the months; light red circle, June; medium-red diamond, July: dark red square, August; orange triangle, September.

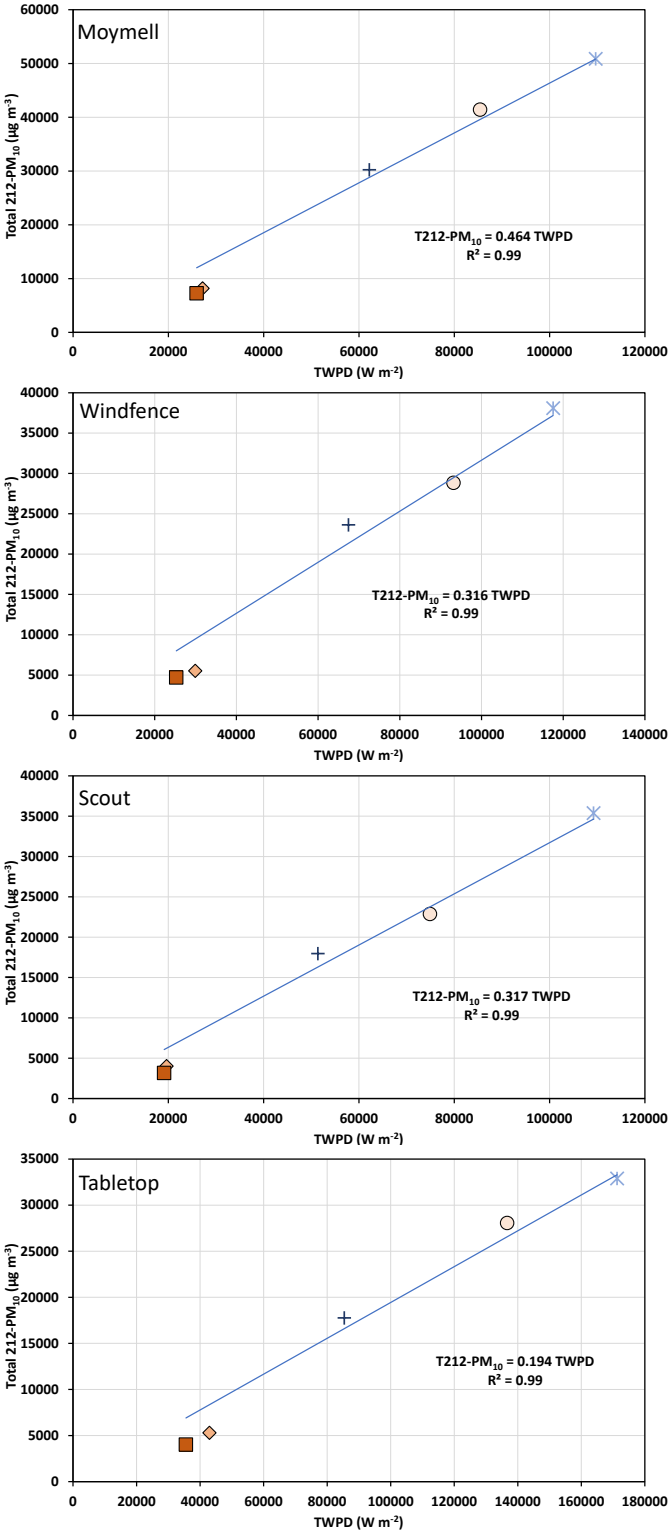

Figure 15. Examples of the T212-PM_{10} and TWPD relation for stations Moymell, Windfence, Scout, and Tabletop for 2020. Shape/color indicates the month; dark blue +, April; light blue ✳, May; light red circle, June; medium-red diamond, July; dark red square, August.

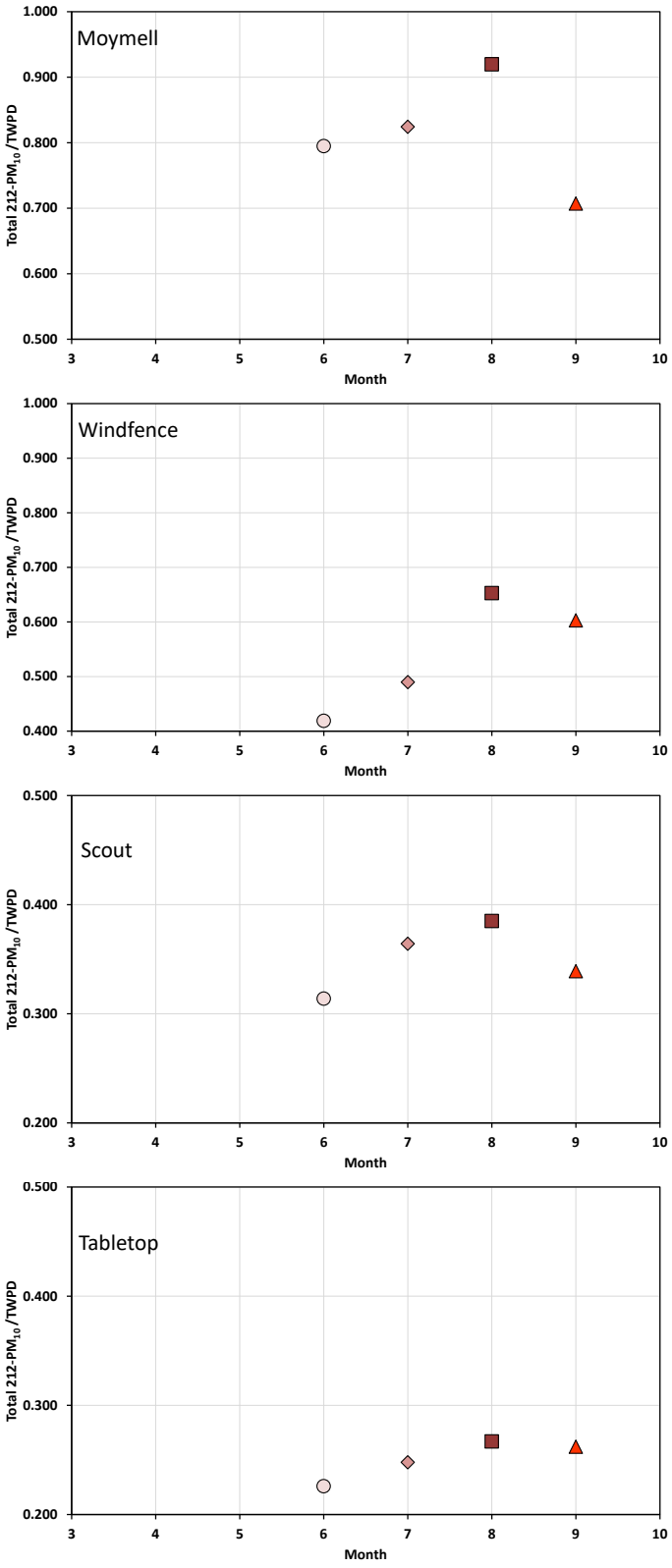

Figure 16. Examples of the T212-PM_{10}:TWPD relation for stations Moymell, Windfence, Scout, and Tabletop for 2019. X-axis number represent month of the year by number, e.g., 6=June.

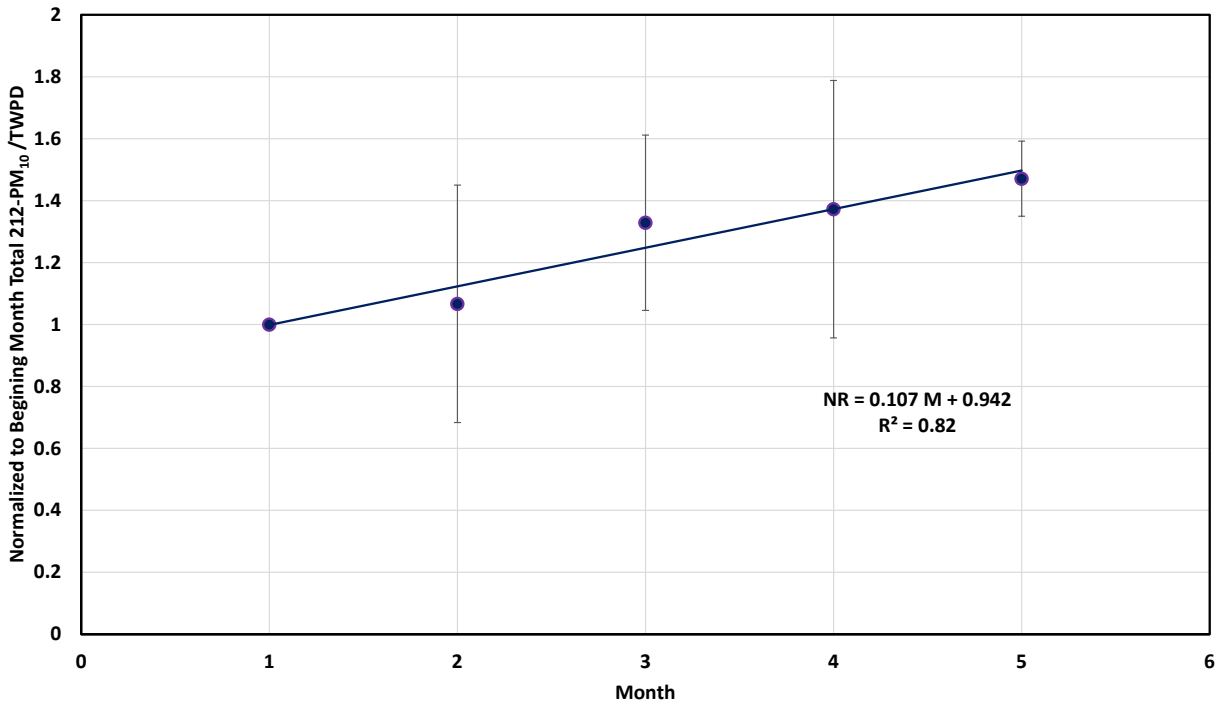

Figure 17. The mean normalized T212-PM_{10}:TWPD ratio as a function of month-long increments of time. Data represent the period from May to September 2019 and include all in-Park stations (see Table 1). Note number on the X-axis does not represent month of the year, as the starting month for the normalization may be May or June.

resulting from saltation created emissions decreased by 46.5% (% change from T212-PM_{10}:TWPD=1 to T212-PM_{10}:TWPD=0.535) between April and August for equivalent conditions of Total WPD, approximately 11.6% each month. This suggests that the cessation of OHV activity has likely allowed the dust emission system to evolve towards a new state representing a less impacted dune system.

The T212-PM_{10}:TWPD values as a function station latitude for 2019 and 2020 are shown in Fig. 21. These data show that the northern stations (latitude >35.005) produced greater concentrations of 212-PM_{10} in 2019 than in 2020, for equivalent WPD values. Of note is the T212-PM_{10}:TWPD ratio for the Lagrande station in 2020 (red circle datum in Fig. 21). This monitoring location has the highest ratio value among all the monitoring stations for all months from April to August, with the mean value, T212-PM_{10}:TWPD=0.805, which is between 2 to 8 times greater than the other stations (Fig. 21). Unfortunately, there was a failure of the MetOne 212-2 unit in 2019 at the Lagrande monitoring station so a direct comparison between 2019 and 2020 is not possible. However, in 2020 the mean T212-

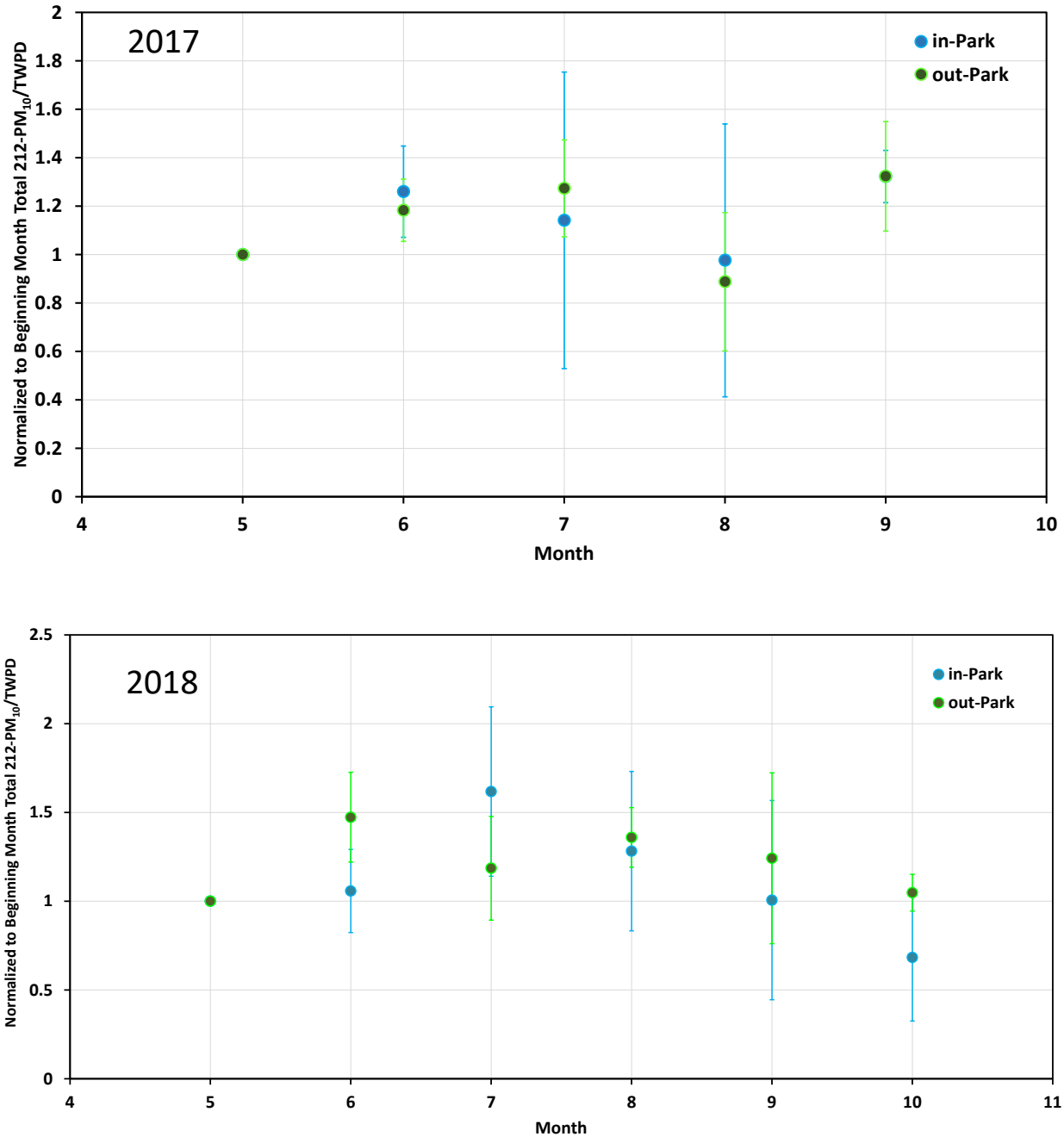

Figure 18. The mean normalized T212-PM_{10}:TWPD ratio (normalized to the starting month of monitoring) as a function of month-long increments of time. Data represent the period from May to September/October in either year. Out-of-Park stations are SODAR, P66, and CDF.

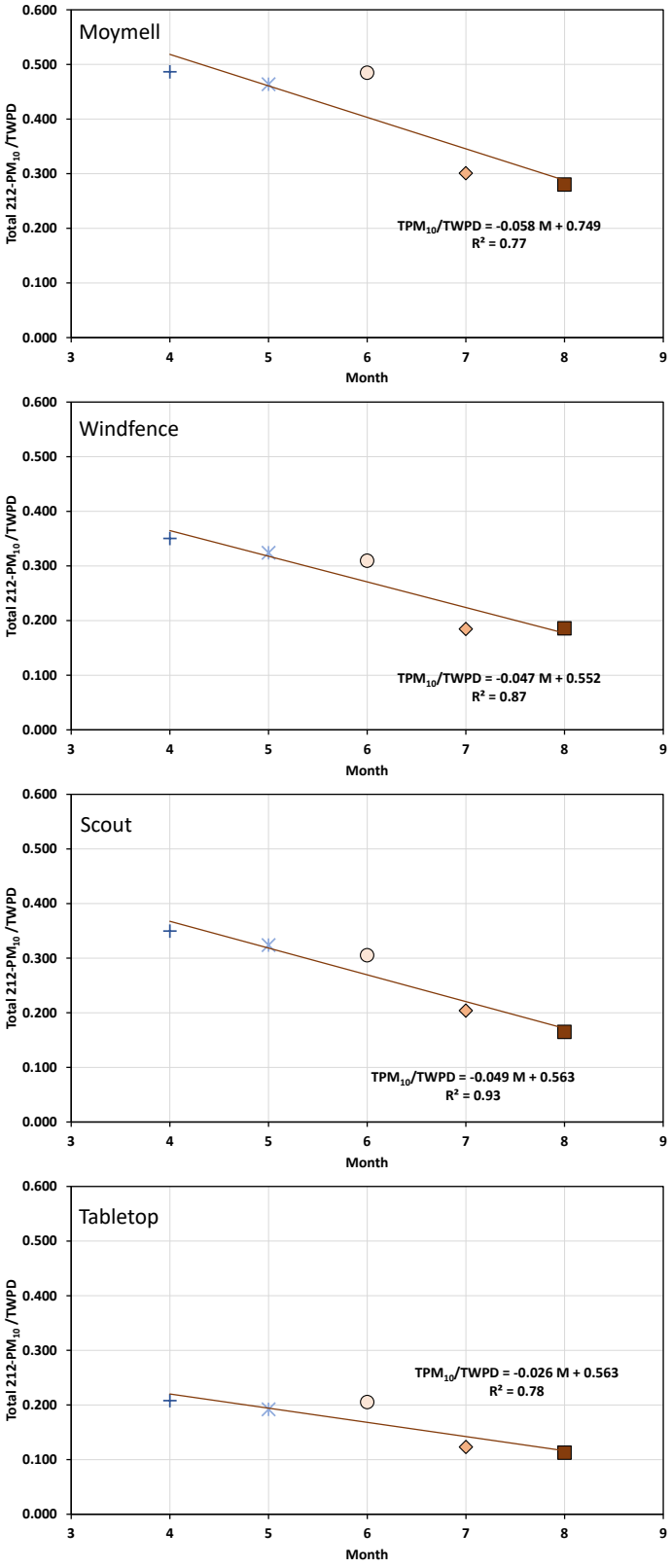

Figure 19. Examples of the T212-PM_{10}:TWPD relation for stations Moymell, Windfence, Scout, and Tabletop for 2020. X-axis number represents month of the year by number, e.g., 4=April.

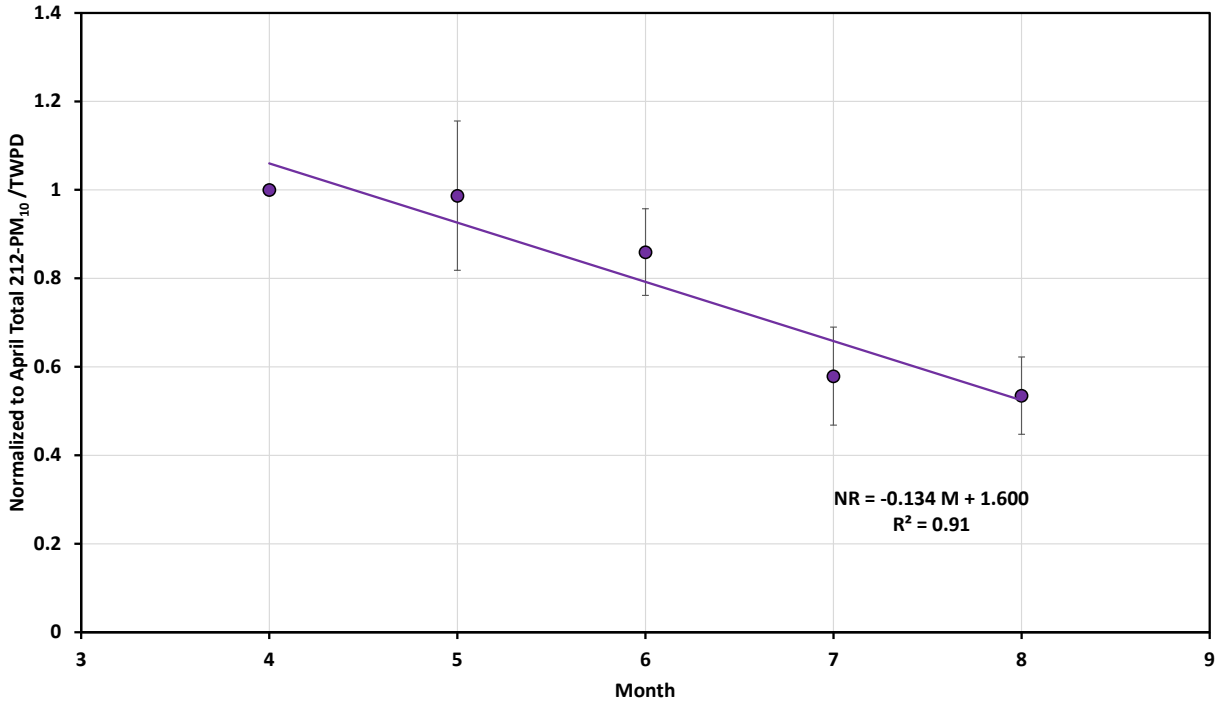

Figure 20. The mean normalized T212-PM_{10}:TWPD ratio as a function of a month-long increments of time. Data represent the period from April to August 2020 and include all in-Park stations (see Table 1).

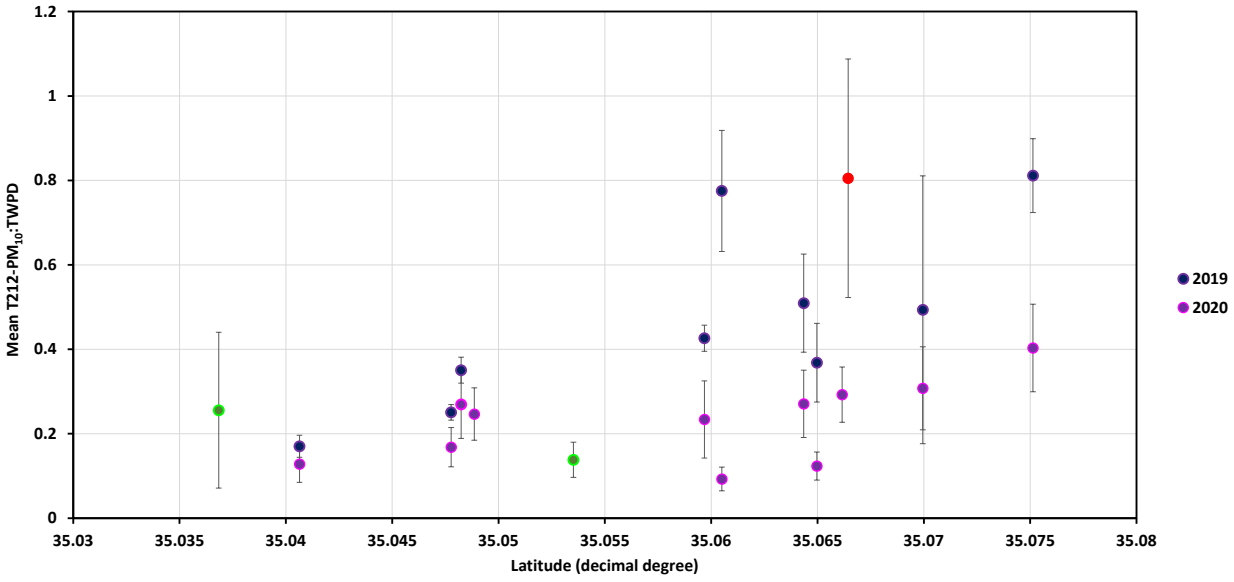

Figure 21. The mean T212-PM_{10}:TWPD ratio for each of the in-Park stations as a function of latitude in 2019 (May or June-Sept) and 2020 (April-Aug). Error bars represent the standard deviation of the mean ratio for the available months of data. The red circle datum marks the Lagrande Tract value in 2020. The green circles are the out-of-Park stations. Green circles are out-of-Park stations (SODAR [35.03684] and Haybale [35.05352], 2020)

PM_{10}:TWPD value for the Lagrande station was in the range reported by nearby stations in 2019. This indicates that the areas upwind of this monitoring station were much more emissive than other parts of the Park in 2020. This is important as emissions from the Lagrande tract impact, to a high degree, the CDF monitoring site.

Since there are no comparable data to define the pattern of TPM_{10}:TWPD across space or through time prior to 2017 and hence for times before OHV activity periods, it is not possible to unambiguously declare the absolute effect of OHV activity on increasing the dune emissivity above a pre-impact condition. The station data from 2019 suggest that on the seasonal time frame May to August, OHV activity increased the saltation-generated PM_{10} concentrations from the dunes by approximately 50% for similar values of WPD (Fig. 17). Upon restriction of OHV activity in 2020, the station data indicate the saltation-generated PM_{10} concentrations from the riding area decreased by approximately 50% from April through to the end of August for similar values of WPD (Fig. 20).

Conclusions

Based on the record of PI-SWERL measurements from 2013 to 2020, and the in-Park monitoring of meteorologic and 212-PM_{10} in 2019 and 2020, it appears that the cessation of OHV activity in 2020 had a demonstrable effect on the emissivity of the dune surfaces in the riding area. In 2019 as OHV activity was unrestricted the PI-SWERL data from across the ODSVRA riding area and the Lagrande Tract, in particular, indicate that emissivity was higher in 2019 than 2020. Although variable through time, due likely to moisture effects on emissivity, the emissivity of the Lagrande Tract by September 2020 was ≈50% less emissive than it was in 2019, according to the PI-SWERL measurements.

The in-Park met-PM stations provide a more continuous record of the dust emissions system across the spatial domain of the ODSVRA than can be obtained with periodic PI-SWERL measurements of emissivity. The instrument network enables characterization of the PM_{10} concentrations through a broad range of environmental conditions in which dust emissions occur. Data from the network indicates that the emissivity of the riding area decreased between April and August in 2020 because PM_{10} concentrations were lower for similar values of WPD. This holds across the entire spatial domain of the monitoring network. It is noted, however, that the Lagrande station, located downwind of the Lagrande Tract, produced much higher PM_{10} concentrations for equivalent WPD values than all the other in-Park stations in 2020. This suggests that the Lagrande tract remained a rich source area for PM_{10} from April-to August 2020. Although the T212-PM_{10}:TWPD ratio for this station did decline through time from April to August similar to all the other stations. The station data from 2020 suggest that the removal of OHV activity in April allowed the dune system to move to a different emissive state that was approximately 50% lower following the passage of four months of time. This correlates with the observed reduction in emissivity in 2020 as measured with the PI-SWERL.

References

Etyemezian, V., J.A. Gillies, M. Shinoda, G. Nikolich, J. King, A.R. Bardis (2014). Accounting for surface roughness on measurements conducted with PI-SWERL: Evaluation of a subjective visual approach and a photogrammetric technique. *Aeolian Research* **13**: 35-50, doi: 10.1016/j.aeolia.2014.003.002.

Etyemezian, V., J.A. Gillies, G. Nikolich, J. Mejia (2019). 2017 and 2018 Aerosol Particle Profiler (APP) Monitoring Network: Summary of Findings. Report prepared by DRI for ODSVRA, California State Parks, September 2019.

Furtak-Cole, E., J.A. Gillies (2020). Wind and PM_{10} Relations Between May/June 2019 and May/June 2020. Report prepared by DRI for ODSVRA, California State Parks, October 2020.

Gillies, J.A., E. Furtak-Cole, V. Etyemezian (2020). Increments of Progress Towards Air Quality Objectives – ODSVRA Dust Controls. Report prepared by DRI for ODSVRA, California State Parks, December 2020.